https://doi.org/10.5194/egusphere-2025-5732
Preprint. Discussion started: 17 December 2025

Explainable Machine Learning diagnosis of Ozone Formation Sensitivity in China: Spatiotemporal Evolution and Driver Attribution

Jinglan Lin[1], Liqing Wu[2], Chujun Chen[1], Yongkang Wu[1], Rui Lin[3], Xuemei Wang[1], Weihua Chen[1*]

[1]College of Environmental and Climate, Jinan University, Guangzhou, 510632, P.R. China
[2]College of Ocean and Meteorology, Guangdong Ocean University, Zhanjiang, 524000, P.R. China
[3]High Performance Computing Department, National Supercomputing Center in Shenzhen, Shenzhen, 518000, P.R. China

Correspondence to: Weihua Chen (chenwh26@jnu.edu.cn)

Abstract. Accurate diagnosis of ozone (O_3) formation sensitivity (OFS) is crucial for effective control strategies, but a long-term, observation-based, interpretable assessment disentangling the roles of meteorology and emissions at the national scale is lacking. This study integrates OMI tropospheric columns of nitrogen dioxide (NO_2) and formaldehyde (HCHO) from 2005 to 2023, using the HCHO/NO_2 ratio (FNR) as a proxy to track the spatiotemporal evolution of OFS in China. We develop an explainable machine learning framework coupling Random Forest (RF) and SHapley Additive exPlanations (SHAP) to quantify the contributions of meteorology and emissions at regional scales. Our findings reveal a policy-driven phase reversal in OFS: from 2005 to 2012, rising NO_2 columns shifted much of China from NO_x-limited to VOC-limited or transitional regimes. Post-2013, the Clean Air Actions led to a decline in NO_2 and a modest increase in HCHO, triggering a nationwide return to NO_x-limited conditions, especially in eastern China. Regionally, the Sichuan Basin (SCB) remained NO_x-limited, the Pearl River Delta (PRD) transitioned rapidly to NO_x-limited, and the Beijing-Tianjin-Hebei (BTH), Yangtze River Delta (YRD), and Fenwei Plain (FWP) showed gradual shifts from VOC- to NO_x-limited regimes. SHAP analysis identifies temperature and surface shortwave radiation as dominant meteorological drivers, while emission patterns vary regionally: non-methane volatile organic compounds (NMVOCs) dominate in BTH, NO_x in PRD, and carbon monoxide (CO) amplifies radical cycling in FWP, YRD, and SCB. These results support a "climate-dominated, emission-modulated" framework for OFS restructuring, offering a transferable diagnostic tool for differentiated O_3 control strategies.

1 Introduction

China has enacted a series of unprecedented clean air policies over the past decade, notably the "Air Pollution Prevention and Control Action Plan (2013–2017)" and the "Three-Year Action Plan for Winning the Blue Sky Defense Battle (2018–2020)" (Chinese State Council, 2013; Chinese State Council, 2018). These measures have driven substantial declines in fine particulate matter ($PM_{2.5}$), yielding stagewise improvements in air quality (Geng et al., 2024; Liu et al., 2024). Yet, in parallel, surface ozone (O_3) has continued to rise (Li et al., 2020; Wei et al., 2022; Wang et al., 2022), emerging as the primary obstacle to

https://doi.org/10.5194/egusphere-2025-5732
Preprint. Discussion started: 17 December 2025

further air quality gains in the post-$PM_{2.5}$ era. In recent years, China has become one of the regions most severely affected by O_3 pollution worldwide (Lu et al., 2018). Major urban clusters such as the Beijing-Tianjin-Hebei (BTH) region, the Yangtze River Delta (YRD), the Pearl River Delta (PRD), the Fenwei Plain (FWP), and the Sichuan Basin (SCB) have experienced persistently elevated O_3 concentrations (Chen et al., 2021; Deng et al., 2022; Guan et al., 2021; Hu et al., 2024), with documented risks to public health and ecosystems (Hua et al., 2025; Liang et al., 2024; Lin et al., 2018).

As a secondary pollutant, O_3 is produced through nonlinear photochemistry involving nitrogen oxides (NO_x = NO + NO_2) and volatile organic compounds (VOCs) under solar radiation (Seinfeld and Pandis, 2016). This nonlinearity implies that O_3 responds differently to changes in NO_x and VOCs across regions and meteorological conditions. Accordingly, O_3 formation sensitivity (OFS) is commonly categorized into NO_x-limited, VOC-limited, and transitional regimes (Duncan et al., 2010; Kleinman, 1994; Martin et al., 2004; Schroeder et al., 2017; Sillman, 1999). Robust identification of OFS and clear attribution of its controlling factors therefore constitute core scientific prerequisites for effective O_3 mitigation and differentiated multi-pollutant control strategies.

Methods for diagnosing OFS have advanced substantially in recent years, and can be broadly classified into model-based methods and observation-based methods (Liu and Shi, 2021), each with distinct strengths and limitations. Among the model-based approaches, typical representatives include source tagging techniques and sensitivity experiments within air quality models. The source tagging techniques determine O_3 formation regimes by tracking precursor contributions (e.g., NO_x and VOCs) via air quality models. For instance, Wu et al. (2022) applied the Community Multiscale Air Quality (CMAQ) model coupled with the O_3 Source Apportionment Technology (OSAT) and showed that OFS across the Pearl River Delta region varied markedly with meteorological conditions. The sensitivity experiments employ atmospheric chemical models (e.g., WRF-Chem and GEOS-Chem) to simulate O_3 response to precursor emission variations, thereby evaluating the effects of precursors on O_3 formation. Using an Observation-Based Model (OBM) coupled with WRF-CMAQ model, Zhang et al. (2024a) demonstrated dynamic shifts in northeastern China from VOC-limited or transitional regimes to NO_x-limited regimes as pollution intensifies. However, both approaches are computationally expensive and tightly constrained by model accuracy, which can hinder broad operational use. By contrast, observation-based photochemical indicator methods offer a simple and computationally efficient alternative that has been widely adopted for regional OFS mapping. These methods use ratios of key photochemical species as regime discriminant. Sillman (1995) first proposed various indicators, such as the hydrogen peroxide (H_2O_2) / nitric acid (HNO_3) ratio, which were later extended to indicators such as O_3 / NO_x and formaldehyde (HCHO) / nitrogen oxides (NO_y = NO_x + HNO_3 + peroxyacetyl nitrate + alkyl nitrates) (Tonnesen et al., 2000). Among them, the satellite-based HCHO / nitrogen dioxide (NO_2) ratio (FNR) has gained prominence for regional-global diagnosis owing to its broad spatiotemporal coverage and strong regional representativeness (Chen et al., 2023; Li et al.,2024; Vazquez Santiago et al., 2024).

Previous studies indicate that over the past two decades, OFS across China has shifted in many regions from VOC-limited toward NO_x-limited or transitional regimes (Du et al., 2022; Itahashi et al., 2022; Johnson et al., 2024). This evolution reflects not only changes in emission structures but also variability in meteorology and climate (Badia et al., 2023; Zhan et al., 2022).

https://doi.org/10.5194/egusphere-2025-5732
Preprint. Discussion started: 17 December 2025

Under ongoing climate change, more frequent extreme heat and enhanced shortwave radiation are expected to further reshape the regional distribution and long-term evolution of OFS (Chen et al., 2020; Vazquez Santiago et al., 2024). Yet, a clear quantitative understanding of how meteorology-emissions interactions jointly regulate OFS remains limited, and national-scale assessments spanning multiple decades are scarce.

To address this gap, we integrate OMI satellite observations of tropospheric NO_2 and HCHO (2005–2023) to characterize the spatiotemporal evolution of O_3 precursors and OFS across China, with explicit comparison of the periods before and after major air-quality policies (2005–2012 vs. 2013–2023). We then couple a Random Forest (RF) model with SHapley Additive exPlanations (SHAP) to quantify the relative contributions of meteorological and emission factors to OFS change. The resulting satellite-constrained, explainable machine learning (ML) diagnostic provides a decomposable and comparable attribution of meteorology versus emissions, advances understanding of regional heterogeneity and long-term mechanisms, and offers a decision-ready basis for region-specific, tiered O_3 control strategies with broader relevance for global O_3 pollution mitigation.

2 Data and methods

2.1 Study area and data sources

2.1.1 Study area

This study spans mainland China, with particular emphasis on five ozone-prone urban clusters: the Beijing-Tianjin-Hebei (BTH) region, the Yangtze River Delta (YRD), the Fenwei Plain (FWP), the Sichuan Basin (SCB), and the Pearl River Delta (PRD) (Fig. 1).

https://doi.org/10.5194/egusphere-2025-5732
Preprint. Discussion started: 17 December 2025

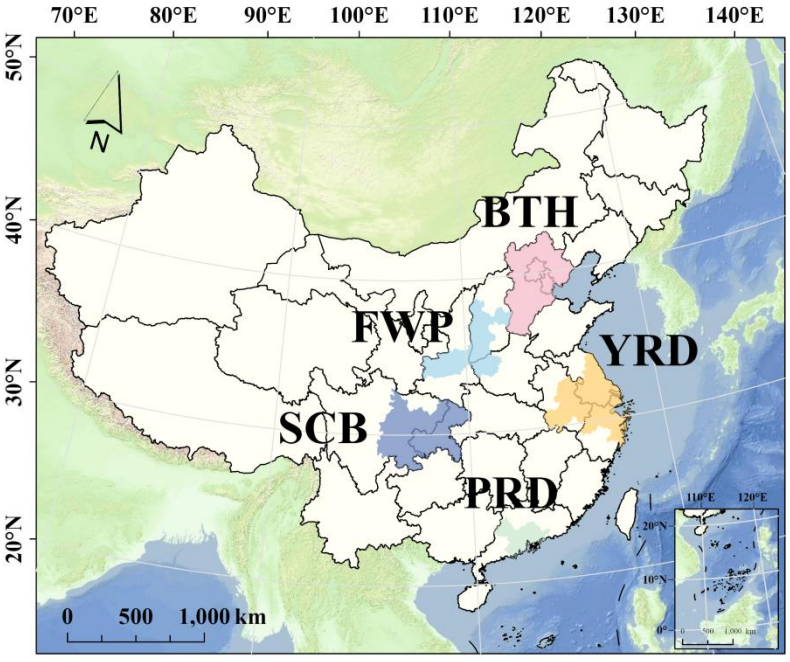

Figure 1. Study domain and five key city clusters: Beijing-Tianjin-Hebei (BTH), Fenwei Plain (FWP), Yangtze River Delta (YRD), Sichuan Basin (SCB), and Pearl River Delta (PRD).

2.1.2 Satellite data

Daily tropospheric NO_2 and HCHO column data from 2005 to 2023 were obtained from the Ozone Monitoring Instrument (OMI) onboard the Aura satellite, accessible via the National Aeronautics and Space Administration (NASA) Goddard Earth Sciences Data and Information Services Center (https://disc.gsfc.nasa.gov, last access: 6 September 2025). The OMI sensor is onboard the Aura Earth observation satellite launched in 2004 (Levelt et al., 2006).

Tropospheric NO_2 data were derived from the OMNO2d Level-3 product, which provides the total tropospheric NO_2 columns under all-sky conditions and, after cloud screening, for cloud fraction < 30%; the native grid is 0.25° × 0.25° with units of molec.cm^{-2} (Krotkov, 2019). Total-column HCHO is obtained from the OMHCHOd product, with a spatial resolution of 0.1° × 0.1° and units of molec.cm^{-2} (Chance, 2019).

Given the short lifetime of HCHO and its predominantly tropospheric burden, total-column HCHO is widely used as a proxy for tropospheric HCHO (Duncan et al., 2010). Nevertheless, clouds can degrade retrieval accuracy below cloud tops (Millet et al., 2006). To ensure quality, we excluded pixels with cloud fraction > 30% and anomalously large HCHO columns (> 1.0 × 10^{17} molec.cm^{-2}), following Zhu et al., (2017). We then applied a 3 × 3 (eight-neighbourhood) moving average to HCHO and resampled the smoothed fields to 0.25° × 0.25° to match the NO_2 grid, following the approach originally applied to SO_2 (Koukouli et al., 2016).

https://doi.org/10.5194/egusphere-2025-5732
Preprint. Discussion started: 17 December 2025

2.1.3 Meteorological data

Meteorological data for 2005–2023 were obtained from the ERA5 reanalysis dataset produced by the European Centre for Medium-Range Weather Forecasts (ECMWF) (Hersbach et al., 2020; https://cds.climate.copernicus.eu/, last access: 14 September 2025). The dataset, originally available at a monthly temporal resolution and 0.25° × 0.25° spatial resolution, was regridded to the OMI-NO_2 grid. This study employs the following meteorological variables for analysis: 2-m temperature (T), relative humidity at 1000 hPa (RH), surface solar radiation downwards (SSRD), 10-m wind speed (WS), surface pressure (SP), and boundary layer height (BLH) (Weng et al., 2022).

2.1.4 Anthropogenic emission data

Anthropogenic emission data for 2005–2023 were obtained from the Multi-resolution Emission Inventory for China (MEIC, http://www.meicmodel.org/, last access: 14 September 2025) developed by Tsinghua University, covering five sectors: power, industry, residential, transportation, and agriculture (Li et al., 2017). MEIC provides ten major species: sulfur dioxide (SO_2), nitrogen oxides (NO_x), carbon monoxide (CO), ammonia (NH_3), carbon dioxide (CO_2), non-methane volatile organic compounds (NMVOCs), fine particulate matter ($PM_{2.5}$), inhalable particles (PM_{10}), black carbon (BC), and organic carbon (OC) (Geng et al., 2024; Zheng et al., 2018). Following Zhang et al. (2024b) and related work linking emissions to O_3 variability via machine learning (ML), we selected monthly emissions of NO_x, NMVOCs, CO, $PM_{2.5}$, and SO_2 as key predictors for diagnosing OFS. All emission data were resampled to 0.25° × 0.25° to match the grid of satellite NO_2 data, ensuring spatial consistency across datasets.

2.2 Methodology

2.2.1 FNR-based ozone formation sensitivity classification

We diagnose OFS using the satellite-based HCHO/NO_2 ratio (FNR), defined as:

$$\mathrm{FNR} = \frac{[HCHO]}{[NO_2]}, \quad (1)$$

where $[HCHO]$ and $[NO_2]$ denote tropospheric columns of HCHO and NO_2, respectively. Following established thresholds (Itahashi et al., 2022; Jin and Holloway, 2015), OFS is classified as: VOC-limited when FNR < 1 (priority control of VOC emissions), NO_x-limited when FNR > 2 (priority control of NO_x emissions), and transitional when 1 ≤ FNR ≤ 2 (coordinated control of VOCs and NO_x).

2.2.2 Trend analysis and statistical testing methods

To quantify the spatiotemporal trends of NO_2 and HCHO columns during 2005–2023, we applied the nonparametric Mann-Kendall (MK) test for trend significance (Hirsch et al., 1982) and the Sen's slope for trend magnitude (Sen, 1968). The MK statistics are computed from all pairwise differences in a time series:

https://doi.org/10.5194/egusphere-2025-5732
Preprint. Discussion started: 17 December 2025

$$S = \sum_{i=1}^{n-1} \sum_{j=i+1}^{n} \mathrm{sgn}(x_j - x_i) , \quad (2)$$

where n is the number of observations, x_i and x_j are values at times i and j, respectively ($j > i$), and $\mathrm{sgn}(\cdot)$ is the sign function that quantifies the direction of change between two observations: it returns 1 when a later value (x_j) is greater than an earlier one (x_i), −1 when it is less, and 0 when they are equal. A positive (negative) S indicates an increasing (decreasing) trend. Statistical significance is assessed using the standardized test statistic Z:

$$Z = \begin{cases} \frac{S-1}{\sqrt{\mathrm{Var}(S)}} & S > 0 \\ 0 & S = 0 \\ \frac{S+1}{\sqrt{\mathrm{Var}(S)}} & S < 0 \end{cases} , \quad (3)$$

where Var(S) represents the variance of the statistic S. When $|Z| \geqslant 1.96$, the trend is considered statistically significant at the 95% confidence level ($p < 0.05$).

Trend magnitude is estimated by the Sen's slope β, defined as the median of all pairwise slopes:

$$\beta = \mathrm{Median}\left(\frac{x_j - x_i}{t_j - t_i}\right) , \quad (4)$$

where t_i and t_j represent the time points of observations i and j, respectively. This MK–Sen framework is distribution-free and robust to outliers, making it well suited to satellite-derived time series.

2.2.3 Machine learning model

Random Forest (RF) is an ensemble machine learning algorithm based on multiple decision trees and is widely used for classification and regression (Breiman, 2001). It implements Bootstrap aggregation (bagging): each tree is trained on a bootstrap replica of the training data with feature randomness at each split, and predictions are combined by majority vote for classification or arithmetic averaging for regression to improve generalization and robustness (Breiman, 1996).

Departing from most studies that regress O_3 concentrations on candidate drivers (Luo et al., 2024; Yao et al., 2024), we frame the problem as classification to identify the key factors distinguishing OFS regimes. In this setting, the RF seeks to minimize overall misclassification. Given an input and an ensemble of trees, the predicted class is the plurality vote:

$$\hat{y} = \mathrm{argmax}_k \sum_{t=1}^{T} \mathrm{I}\left(\mathrm{h}_t(x) = k\right) , \quad (5)$$

where $\mathrm{I}(\cdot)$ is the indicator function, equal to 1 if the t-th tree assigns the sample to class k, and 0 otherwise.

Given regional contrasts in topography, meteorology, and emission structures, we trained separate RF classifiers for each of the five urban clusters (BTH, FWP, YRD, SCB, PRD) to more precisely identify the dominant controls on OFS. Predictors included anthropogenic emissions (NO_x, NMVOCs, CO, $PM_{2.5}$, SO_2) and meteorological parameters (RH, T, SSRD, SP, BLH).

For each region, monthly gridded data for 2005–2023 were split by stratified sampling into 80% training and 20% test sets to preserve the class distribution of VOC-limited, NO_x-limited, and transitional regimes (Pedregosa et al., 2011).

https://doi.org/10.5194/egusphere-2025-5732
Preprint. Discussion started: 17 December 2025

Hyperparameters were optimized via grid search with 10-fold cross-validation; the configuration achieving the highest mean cross-validation (CV) score was retained (Hastie et al., 2009). Tuned parameters included number of decision trees (n_estimators), maximum tree depth (max_depth), minimum samples per leaf (min_samples_leaf), and maximum features per split (max_features), as summarized in Table S1.

Model performance was evaluated using macro-average Accuracy, Precision, Recall, and Fscore (Sokolova and Lapalme, 2009), which can be calculated as follows:

$$\text{Average Accuracy} = \frac{1}{K}\sum_{i=1}^{K}\frac{tp_i+tn_i}{tp_i+fn_i+fp_i+tn_i}, \quad (6)$$

$$\text{Precision}_{\text{m}} = \frac{1}{K}\sum_{i=1}^{K}\frac{tp_i}{tp_i+fp_i}, \quad (7)$$

$$\text{Recall}_{\text{m}} = \frac{1}{K}\sum_{i=1}^{K}\frac{tp_i}{tp_i+fn_i}, \quad (8)$$

$$\text{Fscore}_{\text{m}} = \frac{1}{K}\sum_{i=1}^{K}\frac{2\cdot\text{Precision}_{\text{m}}\cdot\text{Recall}_{\text{m}}}{\text{Precision}_{\text{m}}+\text{Recall}_{\text{m}}}, \quad (9)$$

Here, K denotes the number of classes, i represents the class index, tp_i is the number of true positives, fp_i the number of false positives, fn_i the number of false negatives, and tn_i the number of true negatives for class i.

2.2.4 SHapley Additive exPlanations (SHAP) approach

SHapley Additive exPlanations (SHAP) is an interpretable machine learning framework grounded in cooperative game theory that attributes a model prediction to individual features via Shapley values (Lundberg and Lee, 2017). It is defined as follows:

$$\varphi_i = \sum_{S\subseteq\{1,\dots,n\}\setminus\{i\}}\frac{|S|!(n-|S|-1)!}{n!}[\text{f}(S\cup\{i\})-\text{f}(S)], \quad (10)$$

where φ_i is the SHAP value of feature i, S represents the feature subset excluding feature i, $\text{f}(S\cup\{i\})$ and $\text{f}(S)$ are the model predictions for the corresponding subsets, and $\frac{|S|!(n-|S|-1)!}{n!}$ ensures that the contributions of all feature subsets are fairly distributed. A positive (negative) φ_i indicates that feature i increases (decreases) the predicted class probability or score for the instance considered. By computing SHAP values for each regional RF model, we identify the key features most responsible for discriminating among OFS regimes (NO_x-limited, transitional, VOC-limited) across the five urban clusters.

3 Results and discussion

3.1 Spatiotemporal evolution of ozone precursors

The spatial patterns and long-term trends of tropospheric NO_2 and HCHO columns are shown in Figure 2. NO_2 is highest over densely populated, industrialized urban clusters such as the BTH, YRD, and PRD regions (Fig. 2a), reflecting intensive energy consumption and traffic emissions in eastern China (Fu et al., 2022; Zheng et al., 2018). The annual mean NO_2 column

https://doi.org/10.5194/egusphere-2025-5732
Preprint. Discussion started: 17 December 2025

concentration in BTH (10.71 × 10^{15} molec.cm^{-2} yr^{-1}) is 2.75 times that in SCB (3.89 × 10^{15} molec.cm^{-2} yr^{-1}) (Fig. S1), consistent with heavy industry (e.g., steelmaking) and winter heating by coal (Feng et al., 2014; Li et al., 2010). From 2005 to 2012, nationwide NO_2 increased by 38.9%, with the strongest growth in the east (maximum trend of 1.33 × 10^{15} molec.cm^{-2} yr^{-1}). An exception is the PRD region, where NO_2 already decreased by 9.1% (maximum trend of −1.01 × 10^{15} molec.cm^{-2} yr^{-1}), marking an early turning point attributable to industrial restructuring and vehicular control (Bian et al., 2019; Lu et al., 2020). Following major clean air policies in 2013, NO_2 declined by 19.0% broadly (Fig. 2c), with the steepest decreases in eastern urban clusters, with the maximum reduction reaching −1.35 × 10^{15} molec.cm^{-2} yr^{-1}, confirming policy-driven NO_x reductions (Li et al., 2023; Shah et al., 2020). This inflection is central to subsequent OFS transitions.

In contrast, HCHO columns are elevated not only over eastern urban clusters but also across the southwest regions (e.g., Guangxi, Yunnan, western Sichuan, and southern Tibet), where values can exceed those in the east (Fig. 2d). This distribution aligns with intensified emissions of biogenic VOCs (BVOCs) emissions under warm, high-irradiance conditions. Regionally, the PRD records the highest annual mean HCHO column (9.91 × 10^{15} molec.cm^{-2} yr^{-1}) (Fig. S1), reflecting the combined influence of strong anthropogenic emissions and substantial biogenic contributions (Xia et al., 2024). The temporal evolution of HCHO differs from that of NO_2. During 2005–2012, HCHO exhibited a modest national increase at a rate of 0.13 × 10^{15} molec.cm^{-2} yr^{-1}, corresponding to an 11.4% increase, with the most pronounced growth along the North China–East China urban corridor. From 2013 to 2023, large areas of northwestern China shifted to a clear increasing trend, and the national mean rate rose to 0.15 × 10^{15} molec.cm^{-2} yr^{-1}, corresponding to a 23.7% increase. The sustained post-2013 rise is likely driven by two factors: (1) regional warming and enhanced shortwave radiation that stimulate BVOCs emissions (Wang et al., 2024); and (2) reductions in NO_x emissions that outpaced the reduction in anthropogenic VOCs (AVOCs), altering the photochemical environment and increasing both HCHO production efficiency and atmospheric lifetime. Overall, the persistent increase in HCHO is consistent with the observed rise in surface O_3 over the past decade (Wang et al., 2022; Xia et al., 2024).

In summary, the long-term evolution of O_3 precursors is jointly shaped by policy and climate. NO_x levels declined in direct response to emission controls, whereas the persistent rise in HCHO underscores the climate sensitivity of natural sources.

https://doi.org/10.5194/egusphere-2025-5732
Preprint. Discussion started: 17 December 2025

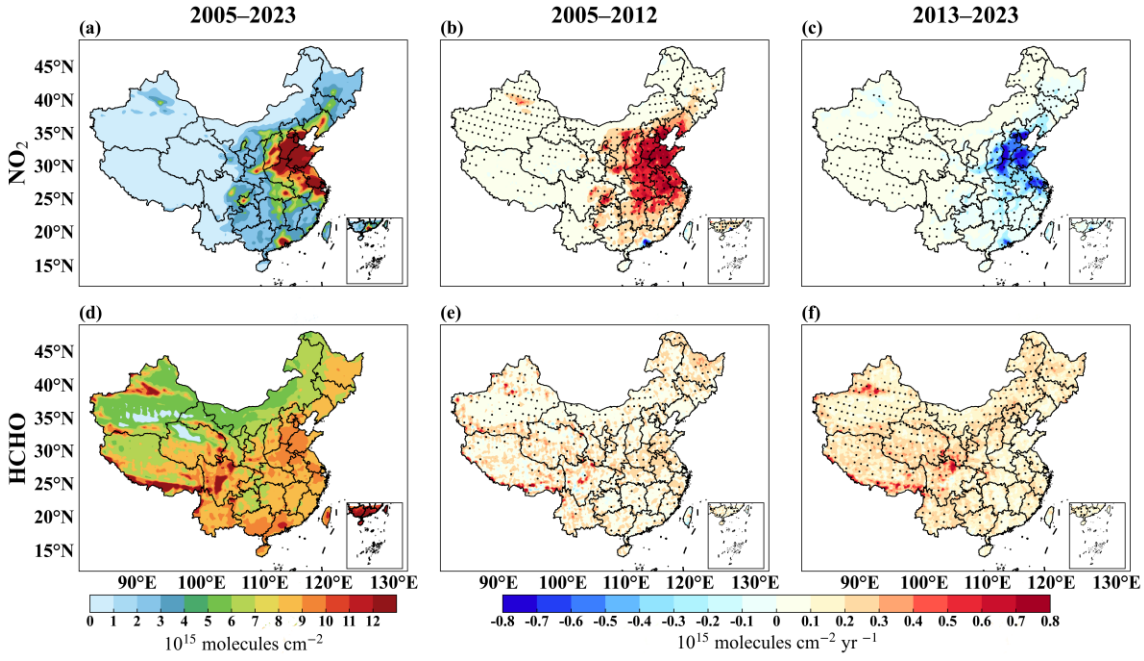

Figure 2. Spatiotemporal variations of tropospheric NO_2 and HCHO columns over China. (a, d) Distribution of annual average columns for 2005–2023; spatial distributions of the Sen's slope and Mann-Kendall (MK) test results for annual means during 2005–2012 (b, e) and 2013–2020 (c, f). Black dots in panels (b, c, e, f) mark grids that pass the MK significance test ($p < 0.05$).

3.2 Spatiotemporal evolution of ozone formation sensitivity regimes

3.2.1 Interannual variations of regional FNR

From 2005 to 2023, interannual variations in FNR differed markedly among China's five major urban clusters (Fig. 3). The SCB exhibited the highest annual mean FNR (3.07) and a modest upward trend (0.02 yr^{-1}), consistent with a persistently NO_x-limited regime. This elevated FNR aligns with the basin's climatic conditions, characterized by high temperature and strong shortwave radiation that enhance BVOCs emissions (Wang et al., 2024). Continued declines in anthropogenic NO_x after 2013 further increased the relative scarcity of NO_x (Yang et al., 2025), reinforcing NO_x limitation. The PRD showed a steeper increase in FNR (0.05 yr^{-1}, $p < 0.001$), rising from 1.83 in 2005 to 2.63 in 2023. This trajectory indicates a shift from VOC-limited or transitional regimes toward NO_x-limited regimes, driven primarily by substantial NO_x reductions from road traffic and industrial sources.

The YRD, BTH, and FWP regions exhibited a U-shaped evolution. Specifically, during 2005–2012, FNR generally declined, indicating movement toward VOC-limited sensitivity. After 2013, FNR increased sharply as NO_2 columns fell and HCHO columns rose moderately, pushing these regions back toward NO_x-limited regimes. This pattern reflects the joint influence of policy and climate. Clean-air measures prioritized NO_x abatement, while regional warming has enhanced the temperature-dependent emissions of both AVOCs and BVOCs, thereby increasing O_3 production efficiency (Pfannerstill et al., 2024; Wu et al., 2024). Together these factors elevated FNR and re-established NO_x-limited regimes.

https://doi.org/10.5194/egusphere-2025-5732
Preprint. Discussion started: 17 December 2025

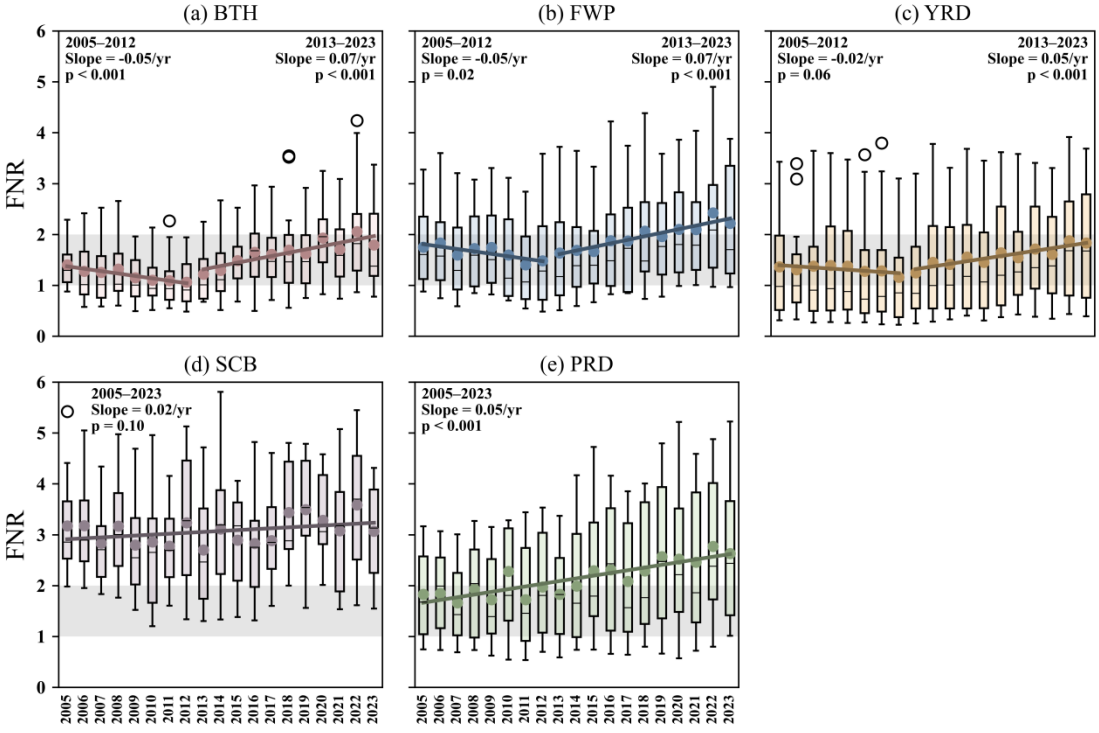

Figure 3. Interannual variations of FNR in key regions during 2005–2023. Box plots show the median (horizontal line), 25th and 75th percentiles (box bounds), minimum and maximum (whiskers), and the mean (plus signs).

3.2.2 Spatial distribution patterns of ozone formation sensitivity regimes

Based on OMI-retrieved FNR, OFS in China during 2005–2023 exhibits a characteristic spatial pattern (Fig. 4): VOC-limited regimes predominate in eastern urban clusters, whereas NO_x-limited regimes are more common in surrounding suburban and less developed areas. In urban clusters such as BTH and YRD, high anthropogenic NO_x emissions depress FNR and yield predominantly VOC-limited regimes in most years. With increasing distance from urban cores, NO_x emissions weaken and the relative contribution of BVOCs rises, producing higher FNR and a shift toward NO_x limitation. This arrangement accords with previous studies and reflects regional contrasts in emission structures, land cover, and urbanization gradients (Chen et al., 2020; Ren et al., 2022).

The areal fractions of OFS regimes exhibit clear phase transitions around the Air Pollution Prevention and Control Action Plan (Fig. 4d). During 2005–2012, China shifted from NO_x-limited toward VOC-limited or transitional regimes: the NO_x-limited fractions fell by 5.4%, while transitional and VOC-limited areas increased by 3.2% and 2.1%, respectively. Although both NO_2 and HCHO columns rose in this period, NO_2 increased more rapidly, lowering FNR and favoring VOC limitation. During 2013–2023, strengthened NO_x emission controls, comparatively slower VOC abatement, and climate-driven enhancements in BVOC emissions collectively elevated FNR and steered the national OFS distribution back toward NO_x limitation. By 2023, VOC-limited regimes accounted for only 0.2%, whereas NO_x-limited regimes expanded to 89.4%. This

https://doi.org/10.5194/egusphere-2025-5732
Preprint. Discussion started: 17 December 2025

inverted U-shaped evolution of OFS underscores the asymmetry in precursor reductions during China's air pollution control process and highlights the combined effects of policy interventions and climatic variability on regional O_3 chemistry.

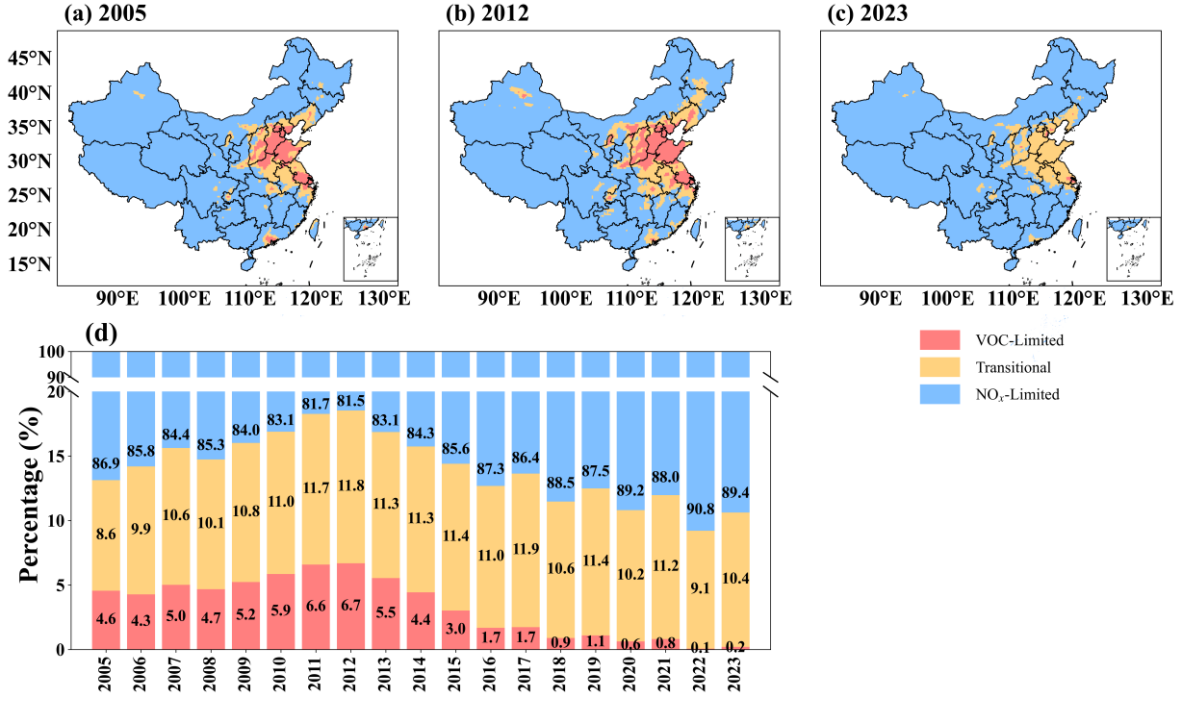

Figure 4. Spatial distributions of FNR over China for (a) 2005, (b) 2012, and (c) 2023; (d) interannual variation in the areal proportion of OFS regimes during 2005–2023.

3.2.3 Seasonal characteristics of ozone formation sensitivity regimes

OFS exhibits marked seasonality (Fig. 5), largely reflecting the distinct seasonal cycles of its precursors, HCHO and NO_2. Specifically, HCHO columns, influenced by BVOCs emissions and photochemical reaction rates (Narumi, 2009; Xue et al., 2022), follow a "summer-high, winter-low" pattern (Fig. S2). In contrast, NO_2 is elevated in winter and depressed in summer, consistent with heating-related emissions and seasonal changes in boundary layer height (Fig. S3) (Bai et al., 2025). The asynchronous variability of these precursors, combined with seasonal meteorology, produces pronounced seasonal shifts in sensitivity across China. The spatial distributions of OFS in spring and autumn are similar, with VOC-limited and transitional regimes mainly concentrated in core urban areas. Due to stronger photochemical activity in autumn (Zhang et al., 2025), the proportion of VOC-limited regimes is slightly higher than in spring, consistent with the findings of Sun et al. (2018a).

In summer, high temperatures and strong shortwave radiation enhance BVOCs emissions, especially in forested and densely vegetated regions of southern China. The same radiative conditions accelerate NO_2 photolysis and weaken O_3 titration, thereby promoting photochemical O_3 production (Pope et al., 2015). Under these high-VOCs, low-NO_x conditions, FNR increases and most regions exhibit NO_x-limited behavior, with the widest spatial extent of NO_x-limited regimes observed in summer.

https://doi.org/10.5194/egusphere-2025-5732
Preprint. Discussion started: 17 December 2025

Winter presents a contrasting regime. Centralized heating and the combustion of coal and diesel substantially increase NO_x emissions, raising NO_2 columns (Fig. S3; Wang et al., 2019). Adverse dispersion conditions, such as low temperatures, weak winds, and a stable boundary layer, further inhibit vertical mixing and dilution (Su et al., 2020; Ahmad et al., 2024), reinforcing NO_2 accumulation. Simultaneously, BVOCs emissions decline as vegetation becomes dormant, and reduced solar radiation lowers photochemical HCHO production, leading to a pronounced decrease in HCHO columns (Fig. S2). FNR correspondingly falls, and the atmosphere shifts toward VOC-limited regimes. Consequently, the spatial extent of VOC-limited areas reaches its annual maximum in winter, encompassing large portions of northeastern, northern, eastern, and southern China.

The seasonal modulation of O_3 sensitivity arises not only from direct changes in precursor abundances but also from nonlinear amplification within the photochemical reaction chain. Elevated summer temperatures accelerate peroxy radicals (HO_2 and RO_2) + NO reactions, increasing radical propagation and O_3 production efficiency (Meng et al., 2023). In winter, despite weaker photochemistry, a shallow boundary layer traps pollutants near the surface (Xiang et al., 2019), intensifying NO titration of O_3 and altering FNR and regime classification. Seasonal evolution of sensitivity regimes therefore reflects the combined effects of emission variability and meteorological control on oxidant levels and reaction pathways.

These dynamics carry clear policy implications. Control strategies should be seasonally differentiated. In summer, priority should be given to NO_x reductions to avoid enhancing O_3 under NO_x-limited conditions. In winter, coordinated VOCs controls, particularly from evaporative anthropogenic sources such as solvents and fuel evaporation, are needed to mitigate VOCs limitation and facilitate O_3 abatement. Looking ahead, projected increases in BVOCs emissions under climate warming (Liu et al., 2019) underscore the need for adaptive, region- and season-specific strategies that couple sensitivity diagnostics with synergistic precursor reductions.

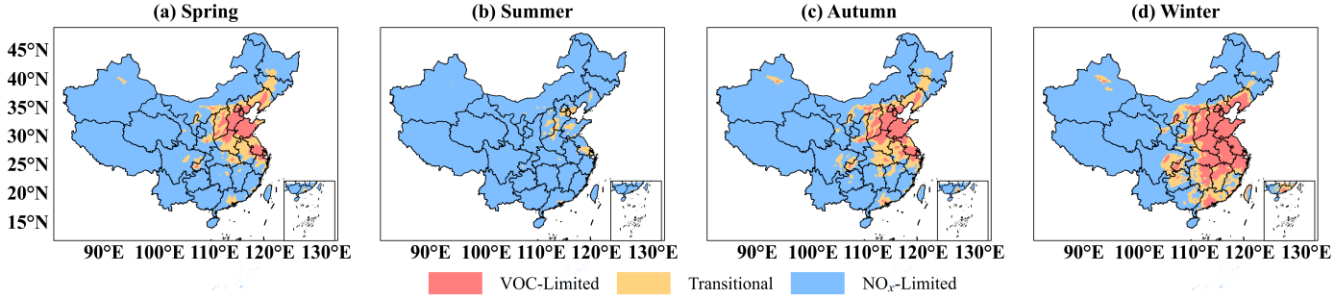

Figure 5. Seasonal distribution of OFS regimes over China from 2005 to 2023.

3.2.4 Impact of short-term COVID-19 lockdown on ozone formation sensitivity regimes

The nationwide COVID-19 lockdown in early 2020 produced a sharp, short-lived reduction in anthropogenic emissions and provided a quasi-experiment to examine the response of OFS to abrupt emission perturbations. We stratified this interval into three phases: pre-lockdown (January 1–22, 2020; 22 days), during-lockdown (January 23–February 13, 2020; 22 days), and post-lockdown (February 14–March 7, 2020; 23 days).

https://doi.org/10.5194/egusphere-2025-5732
Preprint. Discussion started: 17 December 2025

Figure 6 displays the spatial distributions of O_3 precursors and the FNR across these phases. Before the lockdown, a continuous belt of elevated tropospheric NO_2 columns extended along the urban-industrial corridor spanning North, East, and South China. During the strict lockdown, both the spatial extent and intensity of high NO_2 declined markedly, consistent with curtailed industrial activity and transportation. In the post-lockdown phase, areas with elevated NO_2 columns rebounded partially, although levels remained below pre-lockdown conditions (Qiao et al., 2022; Zhao et al., 2022). HCHO generally tracked the NO_2 evolution. However, during the post-lockdown phase, HCHO columns increased over South and Southwest China. This rise reflects the combined influences of intensified wildfire emissions from Myanmar and northern Vietnam and enhanced BVOCs emissions (Stavrakou et al., 2021). These patterns indicate that seasonal BVOCs emissions substantially elevated HCHO and, by increasing FNR, shifted OFS toward more NO_x-limited conditions.

Before the lockdown, major eastern urban regions were dominated by VOC-limited or transitional regimes. During the strict lockdown period, the sharp decline in NO_2 elevated the FNR and led to a broad expansion of NO_x-limited conditions. The PRD and YRD regions showed the fastest and most pronounced shift from VOC-limited to NO_x-limited regimes. This shift is consistent with rapid NO_x reduction that weakened urban O_3 titration, leaving O_3 production constrained by the diminished NO_x supply. In contrast, the SCB remained largely NO_x-limited throughout, although its core cities, Chengdu and Chongqing, persisted in VOC-limited regimes. During the post-lockdown phase, as NO_x emissions rebounded, the North China Plain and the northern YRD partially reverted to VOC-limited and transitional regimes. The areal extent of these regimes increased relative to the strict lockdown phase but did not return to pre-lockdown coverage.

The pattern of a short-term shock followed by rapid transition and partial rebound is consistent with the phased shifts observed during 2005–2023. Under warmer conditions with stronger solar radiation, reductions in NO_x more readily drive OFS into the NO_x-limited regime, thereby increasing the marginal effectiveness of NO_x control. Conversely, OFS can revert toward VOC-limited or transitional regimes when NO_x rebounds or when BVOCs emissions rise. These dynamics imply that in warm-season urban clusters, deeper NO_x cuts are likely to deliver more reliable O_3 reductions. In winter and in northern regions affected by space heating, coordinated VOCs control is required to prevent regime reversal and O_3 rebound. Urban greening plans and industrial restructuring should also evaluate the climate-amplified effects of BVOCs to avoid unintended increase in O_3 formation potential.

https://doi.org/10.5194/egusphere-2025-5732
Preprint. Discussion started: 17 December 2025

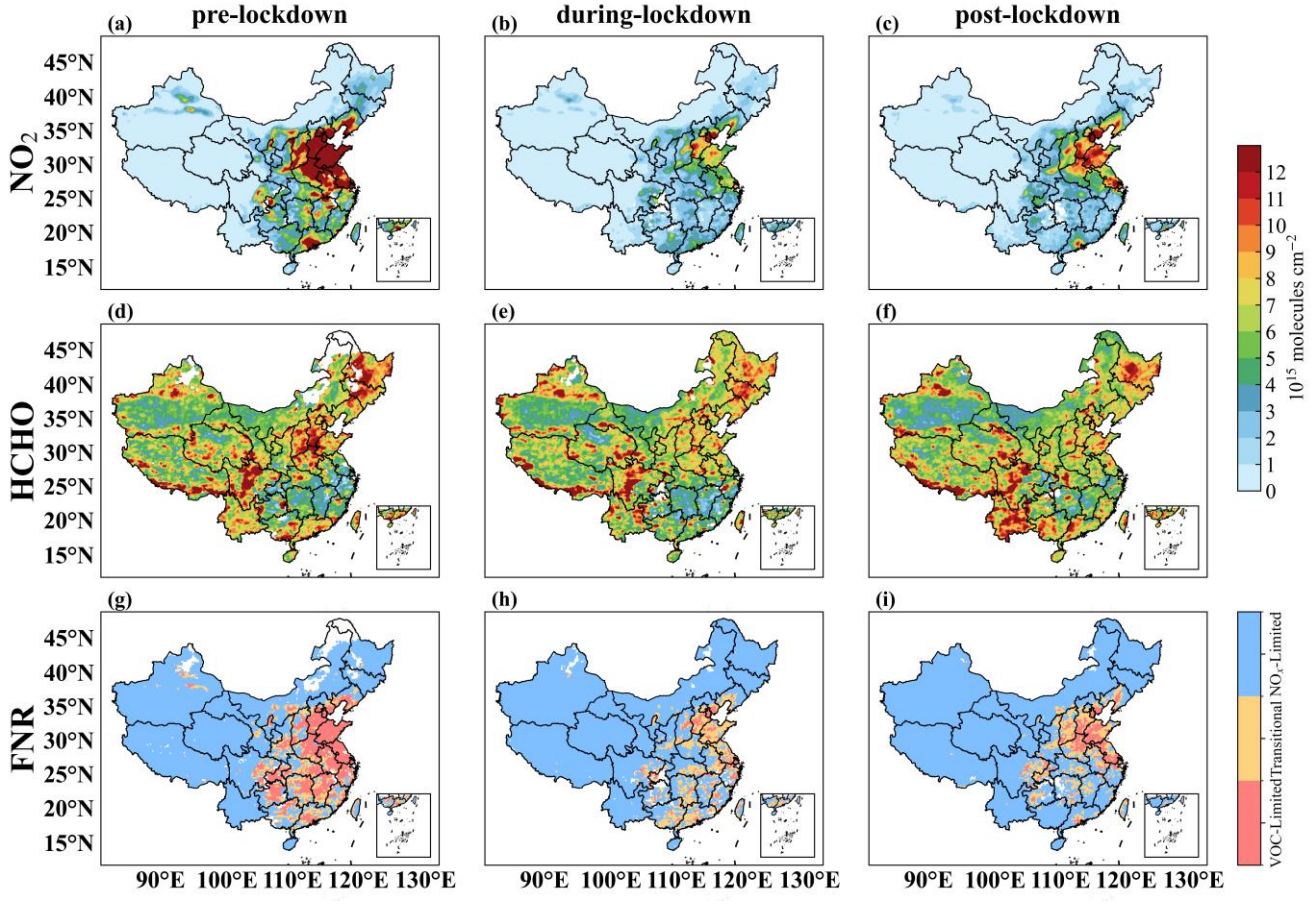

Figure 6. Spatial patterns of tropospheric NO_2 and HCHO columns, and FNR during the pre-, during-, and post- lockdown phases of early 2020.

3.3 Drivers and regional differences of ozone formation sensitivity

Identifying the drivers of OFS is essential for designing regionally tailored and forward-looking emission controls. SHAP analysis of the random forest model indicates that meteorological factors explain substantially more variance than emission-related factors in OFS classification across the five urban clusters, with contributions (calculated from SHAP values) ranging from 64.6% in BTH to 83.6% in YRD (Fig. 7). This pattern points to the dominance of slowly varying climatic controls in shaping the spatial structure of OFS. Among meteorological predictors, 2 m temperature (T) and surface solar radiation downwards (SSRD) consistently ranked highest, reflecting thermally and radiatively driven modulation of atmospheric oxidation capacity. Surface pressure (SP), as an indicator of atmospheric stability, boundary layer depth, and large-scale subsidence, also ranks highly in most regions. Together, these results suggest that gradual shifts in climate (e.g., warming, increased solar radiation, and changes in stability), regulate photochemical reaction rates, boundary-layer mixing, and pollutant

https://doi.org/10.5194/egusphere-2025-5732
Preprint. Discussion started: 17 December 2025

dilution, thereby shaping the spatial pattern and phase transitions of OFS. Importantly, even if anthropogenic emissions stabilize, systematic meteorological changes can still trigger regime shifts in OFS.

In contrast, emission-related drivers show pronounced regional heterogeneity, reflecting localized OFS responses to source profiles. In the BTH region, NMVOCs emissions contribute most (12.4%), indicating that the complex composition of residential heating, solvent use, and industrial emissions renders O_3 formation highly sensitive to variability in VOCs emissions and prone to regime shifts. In the PRD region, NO_x exerts the strongest influence (10.0%), consistent with extensive NO_x abatement over the past decade and with a tendency of OFS to migrate toward NO_x-limited regimes. In the YRD, SCB, and FWP regions, CO dominates among emission-related drivers, with contributions of 6.2%, 13.7%, and 9.2%, respectively. Mechanistically, under sustained NO_x reductions, CO augments radical propagation through the CO + OH → HO_2 pathway, increasing O_3 production efficiency per unit of NO_x (Ren et al., 2013). This radical amplification highlights the need to re-assess the role of CO in O_3 formation, particularly in low-NO_x environments.

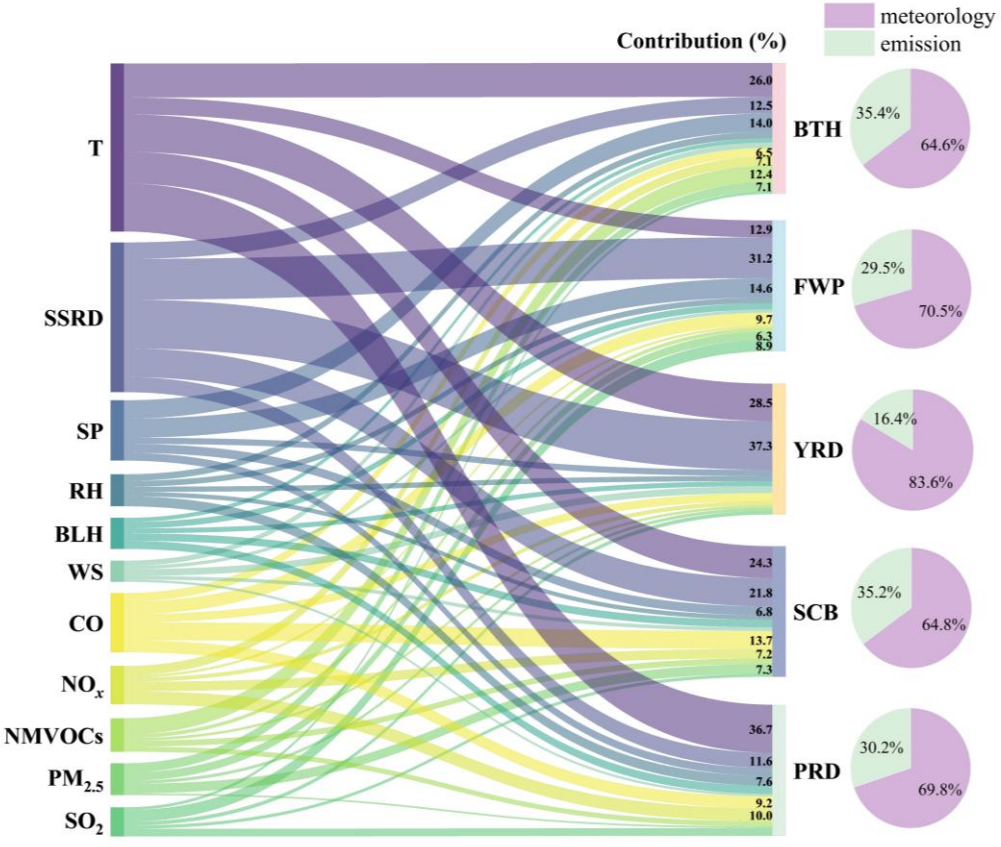

Figure 7. Relative contribution of meteorological and emission factors to OFS classification.

To diagnose the direction and nonlinearity of predictor effects on OFS, we interpreted model outputs for the five urban clusters using SHAP values (Fig. 8). The results indicate that, in NO_x-limited regimes, increases in certain meteorological

https://doi.org/10.5194/egusphere-2025-5732
Preprint. Discussion started: 17 December 2025

factors, particularly T and SSRD, produce positive SHAP values, indicating that warm, strongly irradiated conditions favor classification as NO_x-limited. This behavior is consistent with established mechanisms: higher temperatures accelerate photochemistry and enhance BVOCs emissions, while stronger insolation speeds NO_2 photolysis (Sillman and Samson, 1995). Although many AVOCs sources show weak intrinsic temperature dependence, emissions from evaporative sources (e.g., gasoline) rise sharply at high temperatures, reinforcing this tendency (Rubin et al., 2006). In the BTH and FWP regions, SP contributes strongly; lower SP is associated with synoptic situations that often co-occur with clear skies and intense radiation, thereby pushing the model toward NO_x-limited conditions. By contrast, in VOC-limited regimes, cooler temperature and weaker radiation suppress overall photochemical rates, yielding negative SHAP contributions for T and SSRD and increasing the likelihood of VOC-limited classification. Together, the SHAP patterns reveal regime-dependent, nonlinear responses in which meteorological forcing can shift OFS through changes in oxidant production, radical recycling, and precursor availability.

For emission-related factors, lower levels of NMVOCs, NO_x, CO, and $PM_{2.5}$ are generally associated with higher SHAP values, indicating a greater likelihood of NO_x-limited conditions. Even after NMVOCs levels declined, many areas remain NO_x-limited, implying that other VOCs emissions (e.g., biogenic and residual anthropogenic) are still sufficient to sustain NO_x sensitivity. Because CO emissions often exceed those of NMVOC and NO_x (Sun et al., 2018b), elevated CO can consume atmospheric hydroxyl radicals (·OH) and promote the conversion of NO to NO_2, which strengthens the system's dependence on NO_x (Seinfeld and Pandis, 2016). In addition, reductions in $PM_{2.5}$ decrease the heterogeneous uptake of HO_x and NO_x on particle surfaces, releasing more radicals and reactive nitrogen into the gas phase and increasing the responsiveness of OFS to NO_x (Li et al., 2019). Its SHAP values are high only in the BTH, FWP, and SCB regions, indicating that its impact is mainly concentrated in these areas and relatively weak elsewhere. In summary, higher SHAP values under low precursor levels, high temperature, and strong radiation suggest that NO_x-limited regimes are more likely to persist in relatively clean, photochemically active environment.

By contrast, SHAP contributions in the transitional regime are fragmented and lack a consistent sign, indicating heterogeneous and context-dependent response to both meteorological and emission drivers. Such conditions typically arise where ambient NO_x and VOCs are of comparable magnitude and meteorology is moderate but frequently perturbed, placing the system near a threshold at which small change in drivers can flip the prevailing sensitivity. This near-threshold behavior makes the transitional regime the most uncertain and operationally challenging domain for control, with strongly nonlinear responses and a higher risk of regime reversals. Identifying effective interventions in these areas will require high-resolution mechanistic modeling, ensemble-based scenario analysis, and locally tailored, adaptive management strategies.

Our results indicate heightened sensitivity to NO_x under warm, high insolation conditions. In regions with frequent heat and strong solar radiation, such as the PRD region, NO_x remains the most effective lever for O_3 control even as VOCs levels decline. In BTH, where VOCs variability is large, structural reductions in solvent and industrial VOCs emissions lower the probability of regime shifts. In the YRD, FWP and SCB regions, pronounced CO-driven radical amplification implies that integrated

https://doi.org/10.5194/egusphere-2025-5732
Preprint. Discussion started: 17 December 2025

management of CO and NO_x is needed to mitigate increase in atmospheric oxidizing capacity and in O_3 production efficiency per unit NO_x.

To operationalize these insights, we propose an "FNR–Meteorology–Measures" trigger framework, where the FNR and meteorological forecasts guide control priorities. When FNR rises alongside forecasts of high temperature and clear skies, NO_x measures should be prioritized and tightened. When FNR decreases under milder conditions, coordinated VOCs controls should be deployed. In transitional regimes, NO_x and VOCs control ratios and intervention timing should be adjusted dynamically according to seasonal patterns and expected extreme events. This framework can be integrated with near-surface O_3 forecasting systems, regularly updated emission inventories, and health-risk assessments based on exposure-response functions to enable climate-aware, regionally differentiated governance.

Overall, the spatiotemporal evolution of OFS in China from 2005 to 2023 reflects three primary mechanisms: (1) dominance of slowly varying meteorological drivers, (2) regional modulation by emission structures, and (3) nonlinear responses in co-controlled transitional regimes. These findings provide empirical support for a coupled climate–chemistry–policy framework and offer actionable guidance for optimizing VOCs/NO_x co-reduction pathways under a warming climate.

https://doi.org/10.5194/egusphere-2025-5732
Preprint. Discussion started: 17 December 2025

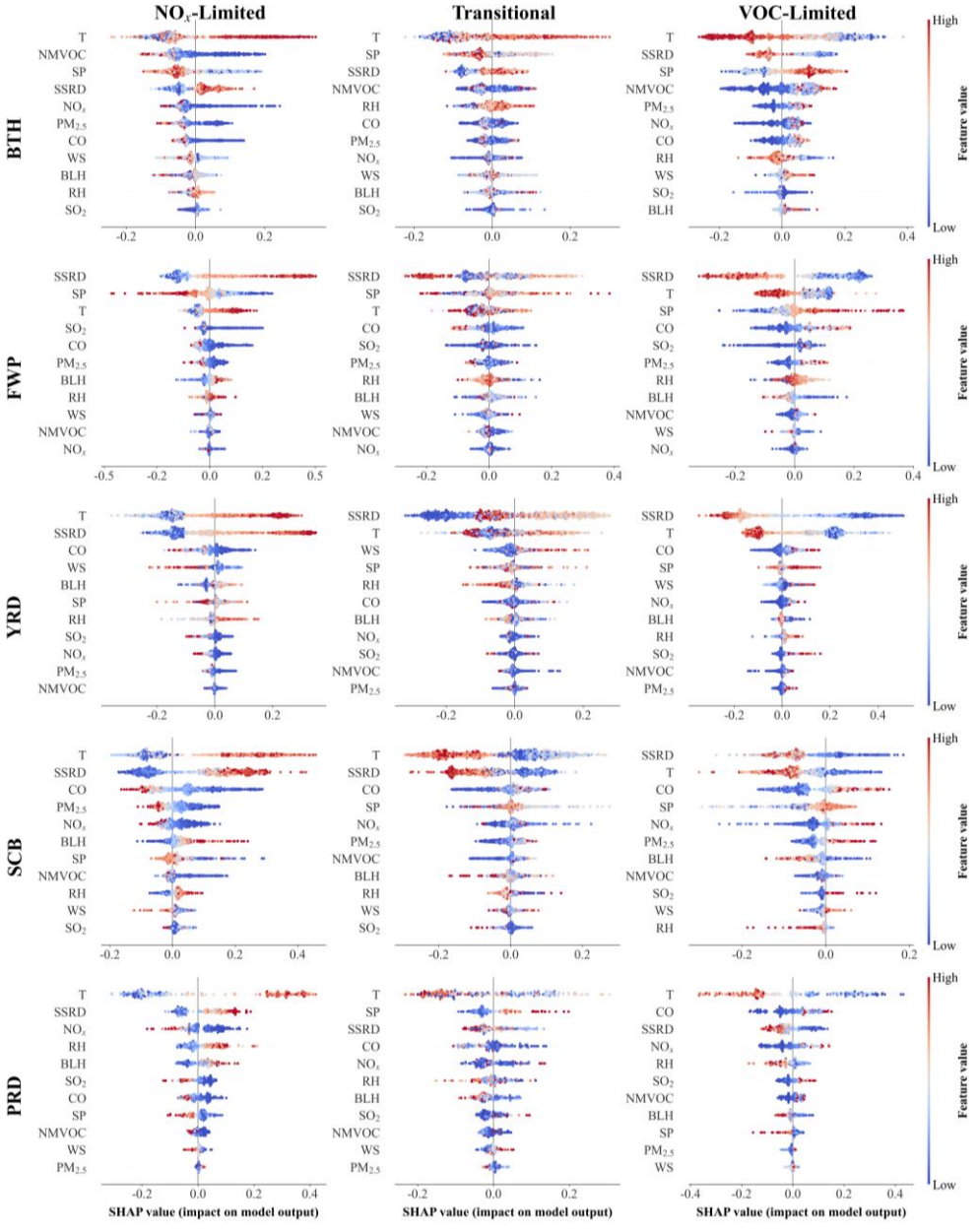

Figure 8. SHAP value distribution in typical urban clusters of China.

4 Conclusion

We combine OMI satellite data (2005–2023) with an explainable machine learning framework (random forest with SHAP attribution) to quantify spatiotemporal evolution of OFS in China under concurrent policy interventions and climatic forcing. Following national clean-air actions, tropospheric NO_2 columns declined markedly while HCHO increased moderately, driving

https://doi.org/10.5194/egusphere-2025-5732
Preprint. Discussion started: 17 December 2025

a national shift in OFS from predominantly VOC-limited or transitional conditions (2005–2012) toward NO_x-limited conditions (2013–2023). Spatial heterogeneity is pronounced: the SCB remained persistently NO_x-limited, the PRD showed the strongest drift toward NO_x-limited conditions and the BTH, YRD, FWP displayed dynamic reversion–transition behavior, confirming phased and regionally distinct evolution.

Model interpretability highlights the dominance of meteorological controls. Temperature (T) and surface solar radiation downwards (SSRD) are the most influential predictors, and surface pressure, a proxy for synoptic stability and boundary-layer structure, also contributes strongly. Emission fingerprints vary by region: NMVOCs contribute most in BTH, NO_x dominates in PRD, and CO acts as a radical amplifier in YRD, SCB, and FWP by enhancing HO_x cycling. The sharp, short-term emission reductions during the COVID-19 lockdown further provide a quasi-natural experiment: rapid NO_2 decline weakened urban O_3 titration and raised the FNR, triggering an abrupt expansion of NO_x-limited conditions in eastern urban areas, followed by only partial reversion post-lockdown.

These lines of evidence indicate that warming and stronger insolation systematically increase the returns to deep NO_x reduction. Nevertheless, coordinated VOCs and CO emissions control remains essential in winter and under high-VOCs conditions, and join assessment of NO_x–VOCs–$PM_{2.5}$ is warranted because declining $PM_{2.5}$ can raise photochemical efficiency. Overall, interactions between climatic variables and rapid emission changes, mediated by radical chemistry, titration balance, and boundary layer structure, govern the long-term evolution and spatial pattern of OFS in China. The satellite-indicator (FNR) and explainable-learning (RF-SHAP) framework enables multiscale, decomposable OFS diagnosis. The resulting "climate-dominated, emission-modulated" paradigm, with transferable and policy-ready criteria, support dynamic rezoning of sensitivity regions and the design of seasonally and regionally differentiated NO_x-VOCs co-reduction pathways, providing methodological support for O_3 control and health co-benefits in megacity regions.

Data availability. Tropospheric NO_2 and HCHO columns for 2005–2023 were obtained from the NASA Goddard Earth Sciences Data and Information Services Center, using the OMNO2d (Krotkov, 2019; https://doi.org/10.5067/Aura/OMI/DATA3009) and OMHCHOd (Chance, 2019; https://doi.org/10.5067/Aura/OMI/DATA3010). Meteorological data were obtained from the ERA5 reanalysis provided by ECMWF via the Copernicus Climate Data Store (Hersbach et al., 2020; https://cds.climate.copernicus.eu/). Anthropogenic emission over China were derived from the Multi-resolution Emission Inventory for China (MEIC; Li et al., 2017; http://www.meicmodel.org/). Specifically, we use the ERA5 monthly averaged data on pressure levels, available at https://doi.org/10.24381/cds.6860a573 (Hersbach et al., 2023a) and ERA5 monthly averaged data on single levels, available at https://doi.org/10.24381/cds.f17050d7 (Hersbach et al., 2023b). All datasets were consistently regridded to a 0.25° × 0.25° spatial resolution for this analysis.

Author contributions. JL, LW and WC designed the research. JL did the data analysis and machine learning work and prepared the draft with support and editing from WC and LW. YW and CC contributed to data analysis. RL and XW contributed to paper revision.

https://doi.org/10.5194/egusphere-2025-5732
Preprint. Discussion started: 17 December 2025

Competing interests. The contact author has declared that none of the authors has any competing interests.

Financial support. This study was supported by the National Key Research and Development Program of China (2023YFC3706205), the National Natural Science Foundation of China (42375109, 42405103), the Guangzhou Basic and Applied Basic Research Foundation (SKXRC2025350, 2023A1515110527).

References

Ahmad, N., Lin, C., Lau, A. K. H., Kim, J., Li, C., Qin, K., Zhao, C., Lin, J., Fung, J. C. H., and Li, Y.: Effects of meteorological conditions on the mixing height of Nitrogen dioxide in China using new-generation geostationary satellite measurements and machine learning, Chemosphere, 346, 140615, https://doi.org/10.1016/j.chemosphere.2023.140615, 2024.

Badia, A., Vidal, V., Ventura, S., Curcoll, R., Segura, R., and Villalba, G.: Modelling the impacts of emission changes on O_3 sensitivity, atmospheric oxidation capacity, and pollution transport over the Catalonia region, Atmos. Chem. Phys., 23, 10751–10774, https://doi.org/10.5194/acp-23-10751-2023, 2023.

Bai, X., Wang, Y., Gui, L., Tao, M., and Zeng, M.: Comparing the influences on NO_2 changes in terms of inter-annual and seasonal variations in different regions of China: meteorological and anthropogenic contributions, Remote Sens., 17, 121, https://doi.org/10.3390/rs17010121, 2025.

Bian, Y., Huang, Z., Ou, J., Zhong, Z., Xu, Y., Zhang, Z., Xiao, X., Ye, X., Wu, Y., Yin, X., Li, C., Chen, L., Shao, M., and Zheng, J.: Evolution of anthropogenic air pollutant emissions in Guangdong Province, China, from 2006 to 2015, Atmos. Chem. Phys., 19, 11701–11719, https://doi.org/10.5194/acp-19-11701-2019, 2019.

Breiman, L.: Bagging Predictors, Mach. Learn., 24, 123–140, https://doi.org/10.1023/A:1018054314350, 1996.

Breiman, L.: Random Forests, Mach. Learn., 45, 5–32, https://doi.org/10.1023/A:1010933404324, 2001.

Chance, K.: OMI/Aura Formaldehyde (HCHO) Total Column Daily L3 Weighted Mean Global 0.1deg Lat/Lon Grid V003, Goddard Earth Sciences Data and Information Services Center (GES DISC) [dataset], Greenbelt, MD, USA, https://doi.org/10.5067/Aura/OMI/DATA3010, 2019.

Chen, Y., Yan, H., Yao, Y., Zeng, C., Gao, P., Zhuang, L., Fan, L., and Ye, D.: Relationships of ozone formation sensitivity with precursors emissions, meteorology and land use types, in Guangdong-Hong Kong-Macao Greater Bay Area, China, J. Environ. Sci., 94, 1–13, https://doi.org/10.1016/j.jes.2020.04.005, 2020.

Chen, Y., Han, H., Zhang, M., Zhao, Y., Huang, Y., Zhou, M., Wang, C., He, G., Huang, R., Luo, B., and Hu, Y.: Trends and variability of ozone pollution over the mountain-basin areas in Sichuan Province during 2013–2020: Synoptic impacts and formation regimes, Atmosphere, 12, 1557, https://doi.org/10.3390/atmos12121557, 2021.

Chen, Y., Wang, M., Yao, Y., Zeng, C., Zhang, W., Yan, H., Gao, P., Fan, L., and Ye, D.: Research on the ozone formation sensitivity indicator of four urban agglomerations of China using Ozone Monitoring Instrument (OMI) satellite data and ground-based measurements, Sci. Total Environ., 869, 161679, https://doi.org/10.1016/j.scitotenv.2023.161679, 2023.

https://doi.org/10.5194/egusphere-2025-5732
Preprint. Discussion started: 17 December 2025

Chinese State Council: Action plan on air pollution prevention and control: http://www.gov.cn/zwgk/2013-09/12/content_2486773.htm, (last accessed: 6 November 2025), 2013 (in Chinese).

Chinese State Council: Three-year action plan on defending the blue Sky: http://www.gov.cn/zhengce/content/2018-07/03/content_5303158.htm, (last accessed: 6 November 2025), 2018 (in Chinese).

Deng, C., Tian, S., Li, Z., and Li, K.: Spatiotemporal characteristics of $PM_{2.5}$ and ozone concentrations in Chinese urban clusters, Chemosphere, 295, 133813, https://doi.org/10.1016/j.chemosphere.2022.133813, 2022.

Du, X., Tang, W., Cheng, M., Zhang, Z., Li, Y., Li, Y., and Meng, F.: Modeling of spatial and temporal variations of ozone-NO_x-VOC sensitivity based on photochemical indicators in China, J. Environ. Sci., 114, 454–464, https://doi.org/10.1016/j.jes.2021.12.026, 2022.

Duncan, B. N., Yoshida, Y., Olson, J. R., Sillman, S., Martin, R. V., Lamsal, L., Hu, Y., Pickering, K. E., Retscher, C., Allen, D. J., and Crawford, J. H.: Application of OMI observations to a space-based indicator of NO_x and VOC controls on surface ozone formation, Atmos. Environ., 44, 2213–2223, https://doi.org/10.1016/j.atmosenv.2010.03.010, 2010.

Feng, X., Li, Q., Zhu, Y., Wang, J., Liang, H., and Xu, R.: Formation and dominant factors of haze pollution over Beijing and its peripheral areas in winter, Atmos. Pollut. Res., 5, 528–538, https://doi.org/10.5094/APR.2014.062, 2014.

Fu, Y., Sun, W., Fan, D., Zhang, Z., and Hao, Y.: An assessment of China's industrial emission characteristics using satellite observations of XCO_2, SO_2, and NO_2, Atmos. Pollut. Res., 13, 101486, https://doi.org/10.1016/j.apr.2022.101486, 2022.

Geng, G., Liu, Y., Liu, Y., Liu, S., Cheng, J., Yan, L., Wu, N., Hu, H., Tong, D., Zheng, B., Yin, Z., He, K., and Zhang, Q.: Efficacy of China's clean air actions to tackle $PM_{2.5}$ pollution between 2013 and 2020, Nat. Geosci., 17, 987–994, https://doi.org/10.1038/s41561-024-01540-z, 2024.

Guan, Y., Xiao, Y., Rong, B., Zhang, N., and Chu, C.: Long-term health impacts attributable to $PM_{2.5}$ and ozone pollution in China's most polluted region during 2015–2020, J. Clean. Prod., 321, 128970, https://doi.org/10.1016/j.jclepro.2021.128970, 2021.

Hastie, T., Tibshirani, R., and Friedman, J.: Model Assessment and Selection, in: The Elements of Statistical Learning. Springer Series in Statistics, Springer, New York, NY, 219–259, https://doi.org/10.1007/978-0-387-84858-7_7, 2009.

Hersbach, H., Bell, B., Berrisford, P., Hirahara, S., Horányi, A., Muñoz-Sabater, J., Nicolas, J., Peubey, C., Radu, R., Schepers, D., Simmons, A., Soci, C., Abdalla, S., Abellan, X., Balsamo, G., Bechtold, P., Biavati, G., Bidlot, J., Bonavita, M., De Chiara, G., Dahlgren, P., Dee, D., Diamantakis, M., Dragani, R., Flemming, J., Forbes, R., Fuentes, M., Geer, A., Haimberger, L., Healy, S., Hogan, R. J., Hólm, E., Janisková, M., Keeley, S., Laloyaux, P., Lopez, P., Lupu, C., Radnoti, G., de Rosnay, P., Rozum, I., Vamborg, F., Villaume, S., and Thépaut, J.-N.: The ERA5 global reanalysis, Quarterly Journal of the Royal Meteorological Society, 146, 1999–2049, https://doi.org/10.1002/qj.3803, 2020.

Hersbach, H., Bell, B., Berrisford, P., Biavati, G., Horányi, A., Muñoz Sabater, J., Nicolas, J., Peubey, C., Radu, R., Rozum, I., Schepers, D., Simmons, A., Soci, C., Dee, D., and Thépaut, J-N.: ERA5 monthly averaged data on pressure levels from 1940 to present, Copernicus Climate Change Service (C3S) Climate Data Store (CDS) [dataset], Reading, UK, https://doi.org/10.24381/cds.6860a573, 2023a.

https://doi.org/10.5194/egusphere-2025-5732
Preprint. Discussion started: 17 December 2025

Hersbach, H., Bell, B., Berrisford, P., Biavati, G., Horányi, A., Muñoz Sabater, J., Nicolas, J., Peubey, C., Radu, R., Rozum, I., Schepers, D., Simmons, A., Soci, C., Dee, D., and Thépaut, J-N.: ERA5 monthly averaged data on single levels from 1940 to present, Copernicus Climate Change Service (C3S) Climate Data Store (CDS) [dataset], Reading, UK, https://doi.org/10.24381/cds.f17050d7, 2023b.

Hirsch, R. M., Slack, J. R., and Smith, R. A.: Techniques of trend analysis for monthly water quality data, Water Resour. Res., 18, 107–121, https://doi.org/10.1029/WR018i001p00107, 1982.

Hu, T., Lin, Y., Liu, R., Xu, Y., Ouyang, S., Wang, B., Zhang, Y., and Liu, S. C.: What caused large ozone variabilities in three megacity clusters in eastern China during 2015–2020?, Atmos. Chem. Phys., 24, 1607–1626, https://doi.org/10.5194/acp-24-1607-2024, 2024.

Hua, Q., Meng, X., Chen, W., Xu, Y., Xu, R., Shi, Y., Li, J., Meng, X., Li, A., Chai, Q., Sheng, M., Yao, Y., Fan, Y., Qiao, R., Zhang, Y., Wang, T., Zhang, Y., Cui, X., Yu, Y., Li, H., Tang, R., Yan, M., Duo, B., Dunzhu, D., Ga, Z., Hou, L., Liu, Y., Shang, J., Chen, Q., Qiu, X., Ye, C., Gong, J., and Zhu, T.: Associations of short-term ozone exposure with hypoxia and arterial stiffness, J. Am. Coll. Cardiol., 85, 606–621, https://doi.org/10.1016/j.jacc.2024.11.044, 2025.

Itahashi, S., Irie, H., Shimadera, H., and Chatani, S.: Fifteen-Year trends (2005–2019) in the satellite-derived ozone-sensitive regime in East Asia: A gradual shift from VOC-sensitive to NO_x-sensitive, Remote Sens., 14, 4512, https://doi.org/10.3390/rs14184512, 2022.

Jin, X. and Holloway, T.: Spatial and temporal variability of ozone sensitivity over China observed from the Ozone Monitoring Instrument, J. Geophys. Res.-Atmos., 120, 7229–7246, https://doi.org/10.1002/2015JD023250, 2015.

Johnson, M. S., Philip, S., Meech, S., Kumar, R., Sorek-Hamer, M., Shiga, Y. P., and Jung, J.: Insights into the long-term (2005–2021) spatiotemporal evolution of summer ozone production sensitivity in the Northern Hemisphere derived with the Ozone Monitoring Instrument (OMI), Atmos. Chem. Phys., 24, 10363–10384, https://doi.org/10.5194/acp-24-10363-2024, 2024.

Kleinman, L. I.: Low and high NO_x tropospheric photochemistry, J. Geophys. Res.-Atmos., 99, 16831–16838, https://doi.org/10.1029/94JD01028, 1994.

Koukouli, M. E., Balis, D. S., van der A, R. J., Theys, N., Hedelt, P., Richter, A., Krotkov, N., Li, C., and Taylor, M.: Anthropogenic sulphur dioxide load over China as observed from different satellite sensors, Atmos. Environ., 145, 45–59, https://doi.org/10.1016/j.atmosenv.2016.09.007, 2016.

Krotkov, N. A., Lamsal, L. N., Marchenko, S. V., Celarier, E. A., Bucsela, E. J., Swartz, W. H., Joiner, J., and the OMI core team: OMI/Aura NO_2 Cloud-Screened Total and Tropospheric Column L3 Global Gridded 0.25 degree × 0.25 degree V3, NASA Goddard Space Flight Center, Goddard Earth Sciences Data and Information Services Center (GES DISC) [dataset], Greenbelt, MD, USA, https://doi.org/10.5067/Aura/OMI/DATA3007, 2019.

Levelt, P. F., Oord, G. H. J. v. d., Dobber, M. R., Malkki, A., Huib, V., Johan de, V., Stammes, P., Lundell, J. O. V., and Saari, H.: The ozone monitoring instrument, IEEE Trans. Geosci. Remote Sens., 44, 1093–1101, https://doi.org/10.1109/TGRS.2006.872333, 2006.

https://doi.org/10.5194/egusphere-2025-5732
Preprint. Discussion started: 17 December 2025

Li, C., Q. Zhang, N. A. Krotkov, D. G. Streets, K. He, S.-C. Tsay, and J. F. Gleason: Recent large reduction in sulfur dioxide emissions from Chinese power plants observed by the Ozone Monitoring Instrument, Geophys. Res. Lett., 37, L08807, https://doi.org/10.1029/2010GL042594, 2010.

Li, M., Liu, H., Geng, G., Hong, C., Liu, F., Song, Y., Tong, D., Zheng, B., Cui, H., Man, H., Zhang, Q., and He, K.: Anthropogenic emission inventories in China: a review, Natl. Sci. Rev., 4, 834–866, https://doi.org/10.1093/nsr/nwx150, 2017.

Li, K., Jacob, D. J., Liao, H., Shen, L., Zhang, Q., and Bates, K. H.: Anthropogenic drivers of 2013–2017 trends in summer surface ozone in China, Proc. Natl. Acad. Sci., 116, 422–427, https://doi.org/10.1073/pnas.1812168116, 2019.

Li, K., Jacob, D. J., Shen, L., Lu, X., De Smedt, I., and Liao, H.: Increases in surface ozone pollution in China from 2013 to 2019: anthropogenic and meteorological influences, Atmos. Chem. Phys., 20, 11423–11433, https://doi.org/10.5194/acp-20-11423-2020, 2020.

Li, S., Wang, S., Wu, Q., Zhang, Y., Ouyang, D., Zheng, H., Han, L., Qiu, X., Wen, Y., Liu, M., Jiang, Y., Yin, D., Liu, K., Zhao, B., Zhang, S., Wu, Y., and Hao, J.: Emission trends of air pollutants and CO_2 in China from 2005 to 2021, Earth Syst. Sci. Data, 15, 2279–2294, https://doi.org/10.5194/essd-15-2279-2023, 2023.

Li, Y., Yu, C., Tao, J., Lu, X., and Chen, L.: Analysis of Ozone Formation Sensitivity in Chinese Representative Regions Using Satellite and Ground-Based Data, Remote Sens., 16, 316, https://doi.org/10.3390/rs16020316, 2024.

Liang, S., Chen, Y., Sun, X., Dong, X., He, G., Pu, Y., Fan, J., Zhong, X., Chen, Z., Lin, Z., Ma, W., and Liu, T.: Long-term exposure to ambient ozone and cardiovascular diseases: Evidence from two national cohort studies in China, J. Adv. Res., 62, 165–173, https://doi.org/10.1016/j.jare.2023.08.010, 2024.

Lin, Y., Jiang, F., Zhao, J., Zhu, G., He, X., Ma, X., Li, S., Sabel, C. E., and Wang, H.: Impacts of O_3 on premature mortality and crop yield loss across China, Atmos. Environ., 194, 41–47, https://doi.org/10.1016/j.atmosenv.2018.09.024, 2018.

Liu, S., Xing, J., Zhang, H., Ding, D., Zhang, F., Zhao, B., Sahu, S. K., and Wang, S.: Climate-driven trends of biogenic volatile organic compound emissions and their impacts on summertime ozone and secondary organic aerosol in China in the 2050s, Atmos. Environ., 218, 117020, https://doi.org/10.1016/j.atmosenv.2019.117020, 2019.

Liu, C. and Shi, K.: A review on methodology in O_3-NO_x-VOC sensitivity study, Environ. Pollut., 291, 118249, https://doi.org/10.1016/j.envpol.2021.118249, 2021.

Liu, R., Shao, M., and Wang, Q. g.: Multi-timescale variation characteristics of $PM_{2.5}$ in different regions of China during 2014–2022, Sci. Total Environ., 920, 171008, https://doi.org/10.1016/j.scitotenv.2024.171008, 2024.

Lu, X., Hong, J., Zhang, L., Cooper, O. R., Schultz, M. G., Xu, X., Wang, T., Gao, M., Zhao, Y., and Zhang, Y.: Severe surface ozone pollution in China: A global perspective, Environ. Sci. Technol. Lett., 5, 487–494, https://doi.org/10.1021/acs.estlett.8b00366, 2018.

Lu, X., Chen, Y., Huang, Y., Chen, D., Shen, J., Lin, C., Li, Z., Fung, J. C. H., and Lau, A. K. H.: Exposure and mortality apportionment of $PM_{2.5}$ between 2006 and 2015 over the Pearl River Delta region in southern China, Atmos. Environ., 231, 117512, https://doi.org/10.1016/j.atmosenv.2020.117512, 2020.

https://doi.org/10.5194/egusphere-2025-5732
Preprint. Discussion started: 17 December 2025

Lundberg, S. M. and Lee, S.-I.: A unified approach to interpreting model predictions, in: Proceedings of the 31st International Conference on Neural Information Processing Systems, Long Beach, California, USA2017, https://doi.org/10.48550/arXiv.1705.07874, 2017.

Luo, Z., Lu, P., Chen, Z., and Liu, R.: Ozone concentration estimation and meteorological impact quantification in the Beijing-Tianjin-Hebei region based on machine learning models, Earth Space Sci., 11, e2023EA003346, https://doi.org/10.1029/2023EA003346, 2024.

Martin, R. V., Fiore, A. M., and Van Donkelaar, A.: Space-based diagnosis of surface ozone sensitivity to anthropogenic emissions, Geophys. Res. Lett., 31, https://doi.org/10.1029/2004GL019416, 2004.

Meng, X., Jiang, J., Chen, T., Zhang, Z., Lu, B., Liu, C., Xue, L., Chen, J., Herrmann, H., and Li, X.: Chemical drivers of ozone change in extreme temperatures in eastern China, Sci. Total Environ., 874, 162424, https://doi.org/10.1016/j.scitotenv.2023.162424, 2023.

Millet, D. B., Jacob, D. J., Turquety, S., Hudman, R. C., Wu, S., Fried, A., Walega, J., Heikes, B. G., Blake, D. R., Singh, H. B., Anderson, B. E., and Clarke, A. D.: Formaldehyde distribution over North America: Implications for satellite retrievals of formaldehyde columns and isoprene emission, J. Geophys. Res.-Atmos., 111, https://doi.org/10.1029/2005JD006853, 2006.

Narumi, D., Kondo, A., and Shimoda, Y.: The effect of the increase in urban temperature on the concentration of photochemical oxidants, Atmos. Environ., 43, 2348–2359, https://doi.org/10.1016/j.atmosenv.2009.01.028, 2009.

Pedregosa, F., Varoquaux, G., Gramfort, A., Michel, V., Thirion, B., Grisel, O., Blondel, M., Prettenhofer, P., Weiss, R., Dubourg, V., Vanderplas, J., Passos, A., Cournapeau, D., Brucher, M., Perrot, M., and Duchesnay, É.: Scikit-learn: Machine Learning in Python, J. Mach. Learn. Res., 12, 2825–2830, https://dl.acm.org/doi/10.5555/1953048.2078195, 2011.

Pfannerstill, E. Y., Arata, C., Zhu, Q., Schulze, B. C., Ward, R., Woods, R., Harkins, C., Schwantes, R. H., Seinfeld, J. H., Bucholtz, A., Cohen, R. C., and Goldstein, A. H.: Temperature-dependent emissions dominate aerosol and ozone formation in Los Angeles, Science, 384, 1324–1329, https://doi.org/10.1126/science.adg8204, 2024.

Pope, R. J., Savage, N. H., Chipperfield, M. P., Ordóñez, C., and Neal, L. S.: The influence of synoptic weather regimes on UK air quality: regional model studies of tropospheric column NO_2, Atmos. Chem. Phys., 15, 11201–11215, https://doi.org/10.5194/acp-15-11201-2015, 2015.

Qiao, J., Liu, X., Ma, Q., Li, Y., and Li, J.: Impact of Covid-19 pandemic on atmospheric environment over China: a satellite perspective, in: Proceedings of IGARSS 2022–2022 IEEE International Geoscience and Remote Sensing Symposium, Kuala Lumpur, Malaysia, 17–22 July 2022, 6614–6617, https://doi.org/10.1109/IGARSS46834.2022.9884338, 2022.

Ren, X., van Duin, D., Cazorla, M., Chen, S., Mao, J., Zhang, L., Brune, W. H., Flynn, J. H., Grossberg, N., Lefer, B. L., Rappenglück, B., Wong, K. W., Tsai, C., Stutz, J., Dibb, J. E., Thomas Jobson, B., Luke, W. T., and Kelley, P.: Atmospheric oxidation chemistry and ozone production: Results from SHARP 2009 in Houston, Texas, J. Geophys. Res.-Atmos., 118, 5770–5780, https://doi.org/10.1002/jgrd.50342, 2013.

https://doi.org/10.5194/egusphere-2025-5732
Preprint. Discussion started: 17 December 2025

Ren, J., Guo, F., and Xie, S.: Diagnosing ozone–NO_x–VOC sensitivity and revealing causes of ozone increases in China based on 2013–2021 satellite retrievals, Atmos. Chem. Phys., 22, 15035–15047, https://doi.org/10.5194/acp-22-15035-2022, 2022.

Rubin, J. I., Kean, A. J., Harley, R. A., Millet, D. B., and Goldstein, A. H.: Temperature dependence of volatile organic compound evaporative emissions from motor vehicles, J. Geophys. Res.-Atmos., 111, https://doi.org/10.1029/2005JD006458, 2006.

Schroeder, J. R., Crawford, J. H., Fried, A., Walega, J., Weinheimer, A., Wisthaler, A., Müller, M., Mikoviny, T., Chen, G., Shook, M., Blake, D. R., and Tonnesen, G. S.: New insights into the column CH_2O/NO_2 ratio as an indicator of near-surface ozone sensitivity, J. Geophys. Res.-Atmos., 122, 8885–8907, https://doi.org/10.1002/2017JD026781, 2017.

Seinfeld, J. H. and Pandis, S. N.: Atmospheric Chemistry and Physics: From Air Pollution to Climate Change, John Wiley & Sons, 1152 pp., ISBN 978-1-118-94740-1, 2016.

Sen, P. K.: Estimates of the regression coefficient based on Kendall's tau, J. Am. Stat. Assoc., 63, 1379–1389, https://doi.org/10.1080/01621459.1968.10480934, 1968.

Shah, V., Jacob, D. J., Li, K., Silvern, R. F., Zhai, S., Liu, M., Lin, J., and Zhang, Q.: Effect of changing NO_x lifetime on the seasonality and long-term trends of satellite-observed tropospheric NO_2 columns over China, Atmos. Chem. Phys., 20, 1483–1495, https://doi.org/10.5194/acp-20-1483-2020, 2020.

Sillman, S.: The use of NO_y, H_2O_2, and HNO_3 as indicators for ozone-NO_x-hydrocarbon sensitivity in urban locations, J. Geophys. Res.-Atmos., 100, 14175–14188, https://doi.org/10.1029/94JD02953, 1995.

Sillman, S.: The relation between ozone, NO_x and hydrocarbons in urban and polluted rural environments, Atmos. Environ., 33, 1821–1845, https://doi.org/10.1016/S1352-2310(98)00345-8, 1999.

Sillman, S. and Samson, P. J.: Impact of temperature on oxidant photochemistry in urban, polluted rural and remote environments, J. Geophys. Res.-Atmos., 100, 11497–11508, https://doi.org/10.1029/94JD02146, 1995.

Sokolova, M. and Lapalme, G.: A systematic analysis of performance measures for classification tasks, Inf. Process. Manag., 45, 427–437, https://doi.org/10.1016/j.ipm.2009.03.002, 2009.

Stavrakou, T., Müller, J.-F., Bauwens, M., Doumbia, T., Elguindi, N., Darras, S., Granier, C., Smedt, I. D., Lerot, C., Van Roozendael, M., Franco, B., Clarisse, L., Clerbaux, C., Coheur, P.-F., Liu, Y., Wang, T., Shi, X., Gaubert, B., Tilmes, S., and Brasseur, G.: Atmospheric impacts of COVID-19 on NO_x and VOC levels over China based on TROPOMI and IASI satellite data and modeling, Atmosphere, 12, 946, https://doi.org/10.3390/atmos12080946, 2021.

Su, T., Li, Z., Zheng, Y., Luan, Q., and Guo, J.: Abnormally shallow boundary layer associated with severe air pollution during the COVID-19 lockdown in China, Geophys. Res. Lett., 47, e2020GL090041, https://doi.org/10.1029/2020GL090041, 2020.

Sun, Y., Liu, C., Palm, M., Vigouroux, C., Notholt, J., Hu, Q., Jones, N., Wang, W., Su, W., Zhang, W., Shan, C., Tian, Y., Xu, X., De Mazière, M., Zhou, M., and Liu, J.: Ozone seasonal evolution and photochemical production regime in the polluted troposphere in eastern China derived from high-resolution Fourier transform spectrometry (FTS) observations, Atmos. Chem. Phys., 18, 14569–14583, https://doi.org/10.5194/acp-18-14569-2018, 2018a.

https://doi.org/10.5194/egusphere-2025-5732
Preprint. Discussion started: 17 December 2025

Sun, W., Shao, M., Granier, C., Liu, Y., Ye, C. S., and Zheng, J. Y.: Long-term trends of anthropogenic SO_2, NO_x, CO, and NMVOCs emissions in China, Earth's Future, 6, 1112–1133, https://doi.org/10.1029/2018EF000822, 2018b.

Tonnesen, G. S. and Dennis, R. L.: Analysis of radical propagation efficiency to assess ozone sensitivity to hydrocarbons and NO_x: 2. Long-lived species as indicators of ozone concentration sensitivity, J. Geophys. Res.-Atmos., 105, 9227–9241, https://doi.org/10.1029/1999JD900372, 2000.

Vazquez Santiago, J., Hata, H., Martinez-Noriega, E. J., and Inoue, K.: Ozone trends and their sensitivity in global megacities under the warming climate, Nat. Commun., 15, 10236, https://doi.org/10.1038/s41467-024-54490-w, 2024.

Wang, S., Li, Y., and Haque, M.: Evidence on the impact of winter heating policy on air pollution and its dynamic changes in North China, Sustainability, 11, 2728, https://doi.org/10.3390/su11102728, 2019.

Wang, W., Parrish, D. D., Wang, S., Bao, F., Ni, R., Li, X., Yang, S., Wang, H., Cheng, Y., and Su, H.: Long-term trend of ozone pollution in China during 2014–2020: distinct seasonal and spatial characteristics and ozone sensitivity, Atmos. Chem. Phys., 22, 8935–8949, https://doi.org/10.5194/acp-22-8935-2022, 2022.

Wang, N., Du, Y., Chen, D., Meng, H., Chen, X., Zhou, L., Shi, G., Zhan, Y., Feng, M., Li, W., Chen, M., Li, Z., and Yang, F.: Spatial disparities of ozone pollution in the Sichuan Basin spurred by extreme, hot weather, Atmos. Chem. Phys., 24, 3029–3042, https://doi.org/10.5194/acp-24-3029-2024, 2024.

Wei, J., Li, Z., Li, K., Dickerson, R. R., Pinker, R. T., Wang, J., Liu, X., Sun, L., Xue, W., and Cribb, M.: Full-coverage mapping and spatiotemporal variations of ground-level ozone (O_3) pollution from 2013 to 2020 across China, Remote Sens. Environ., 270, 112775, https://doi.org/10.1016/j.rse.2021.112775, 2022.

Weng, X., Forster, G. L., and Nowack, P.: A machine learning approach to quantify meteorological drivers of ozone pollution in China from 2015 to 2019, Atmos. Chem. Phys., 22, 8385–8402, https://doi.org/10.5194/acp-22-8385-2022, 2022.

Wu, Y.K., Chen, W.H., Yan, F.H., Mao, J.Y., Yuan, B., Wang, W.W., and Wang, X.M.: Nonlinear response relationship between ozone and precursor emissions in the Pearl River Delta region under different transmission channels, Environ. Sci. 43, 160–169, https://doi.org/10.13227/j.hjkx.202104141, 2022 (in Chinese).

Wu, W., Fu, T.-M., Arnold, S. R., Spracklen, D. V., Zhang, A., Tao, W., Wang, X., Hou, Y., Mo, J., Chen, J., Li, Y., Feng, X., Lin, H., Huang, Z., Zheng, J., Shen, H., Zhu, L., Wang, C., Ye, J., and Yang, X.: Temperature-Dependent evaporative anthropogenic VOC emissions significantly exacerbate regional ozone pollution, Environ. Sci. Technol., 58, 5430–5441, https://doi.org/10.1021/acs.est.3c09122, 2024.

Xia, H., Wang, D., Abad, G. G., Yang, X., Zhu, L., Pu, D., Feng, X., Zhang, A., Song, Z., Mo, Y., and Wang, J.: Multi-scale correlation reveals the evolution of socio-natural contributions to tropospheric HCHO over China from 2005 to 2022, Sci. Total Environ., 954, 176197, https://doi.org/10.1016/j.scitotenv.2024.176197, 2024.

Xiang, Y., Zhang, T., Liu, J., Lv, L., Dong, Y., and Chen, Z.: Atmosphere boundary layer height and its effect on air pollutants in Beijing during winter heavy pollution, Atmos. Res., 215, 305-316, https://doi.org/10.1016/j.atmosres.2018.09.014, 2019.

https://doi.org/10.5194/egusphere-2025-5732
Preprint. Discussion started: 17 December 2025

Xue, J., Zhao, T., Luo, Y., Miao, C., Su, P., Liu, F., Zhang, G., Qin, S., Song, Y., Bu, N., and Xing, C.: Identification of ozone sensitivity for NO_2 and secondary HCHO based on MAX-DOAS measurements in northeast China, Environ. Int., 160, 107048, https://doi.org/10.1016/j.envint.2021.107048, 2022.

Yang, X., Ben, B., Wang, W., Long, B., Xie, Y., Wu, K., and Zhang, X.: Fine particulate matter pollution in the Sichuan Basin of China from 2013 to 2020: Sources, emissions, and mortality burden, Environ. Int., 197, 109366, https://doi.org/10.1016/j.envint.2025.109366, 2025.

Yao, T., Ye, H., Wang, Y., Zhang, J., Guo, J., and Li, J.: Kolmogorov-Zurbenko filter coupled with machine learning to reveal multiple drivers of surface ozone pollution in China from 2015 to 2022, Sci. Total Environ., 949, 175093, https://doi.org/10.1016/j.scitotenv.2024.175093, 2024.

Zhan, J., Liu, Y., Ma, W., Zhang, X., Wang, X., Bi, F., Zhang, Y., Wu, Z., and Li, H.: Ozone formation sensitivity study using machine learning coupled with the reactivity of volatile organic compound species, Atmos. Meas. Tech., 15, 1511–1520, https://doi.org/10.5194/amt-15-1511-2022, 2022.

Zhang, Y., Gao, J., Zhu, Y., Liu, Y., Li, H., Yang, X., Zhong, X., Zhao, M., Wang, W., Che, F., Zhou, D., Wang, S., Zhi, G., Xue, L., and Li, H.: Evolution of ozone formation sensitivity during a persistent regional ozone episode in Northeastern China and its implication for a control strategy, Environ. Sci. Technol., 58, 617–627, https://doi.org/10.1021/acs.est.3c03884, 2024a.

Zhang, C., Xie, Y., Shao, M., and Wang, Q. g.: Application of machine learning to analyze ozone sensitivity to influencing factors: A case study in Nanjing, China, Sci. Total Environ., 929, 172544, https://doi.org/10.1016/j.scitotenv.2024.172544, 2024b.

Zhang, K., Chen, Q., Hong, Y., Ji, X., Chen, G., Lin, Z., Zhang, F., Wu, Y., Yi, Z., Zhang, F., Zhuang, M., and Chen, J.: Elucidating contributions of meteorology and emissions to O_3 variations in coastal city of China during 2019–2022: Insights from VOCs sources, Environ. Pollut., 366, 125491, https://doi.org/10.1016/j.envpol.2024.125491, 2025.

Zhao, C., Zhang, C., Lin, J., Wang, S., Liu, H., Wu, H., and Liu, C.: Variations of urban NO_2 pollution during the COVID-19 outbreak and post-epidemic era in China: A synthesis of remote sensing and in situ measurements, Remote Sens., 14, 419, https://doi.org/10.3390/rs14020419, 2022.

Zheng, B., Tong, D., Li, M., Liu, F., Hong, C., Geng, G., Li, H., Li, X., Peng, L., Qi, J., Yan, L., Zhang, Y., Zhao, H., Zheng, Y., He, K., and Zhang, Q.: Trends in China's anthropogenic emissions since 2010 as the consequence of clean air actions, Atmos. Chem. Phys., 18, 14095–14111, https://doi.org/10.5194/acp-18-14095-2018, 2018.

Zhu, L., Mickley, L. J., Jacob, D. J., Marais, E. A., Sheng, J., Hu, L., Abad, G. G., and Chance, K.: Long-term (2005–2014) trends in formaldehyde (HCHO) columns across North America as seen by the OMI satellite instrument: Evidence of changing emissions of volatile organic compounds, Geophys. Res. Lett., 44, 7079–7086, https://doi.org/10.1002/2017GL073859, 2017.